A case study of wave motion above a jet stream flow system observed by an instrumented balloon

Jean Barat, Charles Cot

A case study of wave motion above a jet stream flow system observed by an instrumented balloon

Jean Barat & Charles Cot

Published online: 15 Dec 2016.

Submit your article to this journal ↗

Article views: 113

View related articles ↗

A case study of wave motion above a jet stream flow system observed by an instrumented balloon

By JEAN BARAT,* *Université Paris VI, France* and CHARLES COT, *Service d'Aéronomie du CNRS, B.P. 3, 91370 Verrieres le Buisson, France*

ABSTRACT

An analysis is presented of the data obtained from an instrumented balloon rising through a jet stream. Emphasis is placed on the determination of the vertical atmospheric velocity. The analysis of the temperature and velocity perturbations shows evidence of a wave structure propagating upward. An estimation of the vertical flux of horizontal momentum is given. These preliminary results show clearly the ability of our helisonde to measure wave motions with a vertical velocity as low as 0.1 m s^{-1}. The method allows a direct measurement of wave propagation in the stratosphere.

1. Introduction

Gravity waves are commonly observed in the atmosphere and their importance has been emphasized during the last decade. They can interact with the mean flow (viscous dissipation, Newtonian cooling, critical level, shear instability) and cause velocity changes. Lindzen (1982), Holton (1982) and Matsuno (1982) have proposed such interaction mechanisms to explain the mean circulation of the middle atmosphere.

The experimental study of atmospheric waves can be carried out by using instrumented aircraft (Lilly and Kennedy, 1973), UHF–VHF radars (Rüster et al., 1978), LIDAR (Chanin and Hauchecorne, 1981) or constant level balloons (Massman, 1981). The ability of these methods to obtain measurements in the middle stratosphere is nevertheless limited to large amplitude waves and the observations remain sparse in the 20–35 km altitude range.

Most of the gravity wave sources are in the troposphere and they can be related to orography, to the jet stream (Bertin et al., 1977) or to convective storms (Uccellini, 1975). As they propagate, these waves are capable of exchanging momentum. In order to explore their interaction with the background flow, it is then worthwhile to perform continuous vertical measurements over a broad range of altitudes from the troposphere up to the middle stratosphere.

Lalas and Einaudi (1980) have shown that gravity waves can be detected through the induced vertical variation of the ascent rate of rawinsonde balloons. However, even in the case of constant volume balloons, the relative ascent velocity changes cannot be computed with great accuracy and the method can only be used when the wave motion has large amplitude. During the last few years, we have devised a new balloon-borne instrument, the helisonde, to study gravity waves between 0 and 30 km (Barat and Génie, 1982). The sounding provides, without assumptions about the vertical velocity of the balloon, continuous profiles of temperature, pressure and vertical velocity of the air. With this set of parameters, it is possible to identify wave motions and to calculate some of their characteristics. In this paper, we present typical results obtained during a test flight of the helisonde. A gravity wave motion is observed from above the tropopause up to 26 km. The measurement technique is discussed in the following section. The data set is presented in Section 3 and the analysis is developed in Sections 4 and 5.

---

* Present address: Service d'Aéronomie du CNRS BP 3, 91370 Verrieres le Buisson, France.

2. Measurement technique

2.1. The helisonde

The instrumentation has been described in detail in Barat and Génie (1982) and we include here only the main characteristics of the measurement technique. The helisonde is hung at a distance $h = 160$ m below a zero pressure balloon. During the ascent, an ionic anemometer, located ahead of the helisonde, measures the relative vertical velocity W_R of the gondola with respect to the air. The detection limit of the anemometer, through the telemetry system, is 1 cm s⁻¹. The zero error δW_R is due to mechanical constraints, and varies slowly with altitude but remains always below 0.3 m s⁻¹. The pressure P is sampled every 0.125 s by a metallic capsule. The resolution is limited by the telemetry system which introduces a digitization step δP of 0.06 mb. Two identical microbead thermistors measure the temperature T of the ambient atmosphere every 0.0313 s. The time response τ of the sensors lies between 5 s (1000 mb) and 19 s (25 mb) and the resolution δT through the telemetry device is of 0.03 K.

2.2. The vertical velocity measurement

Assuming that the atmosphere is in a hydrostatic equilibrium, the vertical velocity W_A of the air is given by

$$W_A = W_P - W_R \tag{1}$$

where

$$W_P = -\frac{1}{\rho g}\frac{dP}{dt} \tag{2}$$

is the vertical velocity of the balloon. To calculate W_P from eq. (2), the uniform series of pressure $P(n)$ cannot be used directly because the digitization step δP is of the same order of magnitude as the actual pressure variation $|P(n) - P(n+1)|$. We have therefore filtered $P(n)$ by a running triangular window $f(n)$ defined by

$$f(n) = 1 - \frac{|2n|}{N+1}$$
$$\text{for} \quad -\tfrac{1}{2}(N-1) \leqslant n \leqslant \tfrac{1}{2}(N-1), \tag{3}$$

where $N = 383$. We have calculated W_A in eq. (1)

by using the filtered value

$$W_P^f(n) = -\frac{1}{\rho g}f\frac{d[fP]}{dt} \tag{4}$$

From eq. (4), we have obtained a uniform altitude series of W_P^f every 5 m along the vertical. Due to the filtering, all the variations of W_P^f with vertical scale lower than the filter length $\lambda_c = 0.5 N \bar{W}_p$, $\Delta t = 130$, (Δt is the time sampling interval $= 0.125$ s) are attenuated. As we will see later, this is of little importance for our observations. After the data processing, the accuracy of the W_P^f values which depend on the calibration factor and on the filtering, is about 3 cm s⁻¹.

While the uncertainty of the W_P^f measurement depends on the resolution of the pressure sensor, the W_R measurement is essentially perturbed by the pendular motion of the helisonde with a period of about 12 s (Barat and Génie, 1982). To suppress this effect, we have applied the filter f to the time series of W_R. The residual error is less than 3 cm s⁻¹. The uncertainty of W_R also depends on the calibration of the anemometer and is below 10%. The atmospheric vertical velocity is then calculated by

$$W_A^f = W_P^f - W_R^f. \tag{5}$$

The zero error δW_R has been estimated by assuming that in the stratosphere, over the 14–28 km altitude range, the mean value of W_A is 0:

$$\int_{14,000}^{28,000}(W_P^f - W_R^f - \delta W_R)\,dz' = 0. \tag{6}$$

We have found $\delta W_R = 0.15$ m s⁻¹ while the value measured in the laboratory before the flight was 0.3 m s⁻¹.

In summary, the helisonde enables us to detect after data processing wave motions of vertical wavelengths one order of magnitude above $\lambda_c = 130$ m with a resolution below 10 cm s⁻¹. This accuracy is substantially better than that obtained with instrumented aircraft, especially in the stratosphere.

2.3. The horizontal wind measurement

During the sounding, the helisonde measured the wind shear $d\vec{V}/dz$ between the balloon and the gondola. By integration, it is possible to obtain the wind profile $\vec{V}(z)$ during the sounding (Barat and Génie, 1982). The accuracy of this measurement

depends on the behaviour of the ballon as a wind sensor and we have shown that, in the case of small balloons moving slowly along the vertical, we can have strong confidence in the method (Barat, 1982). During the test flight detailed here, a 87,000 m^3 balloon was used. With an ascent velocity of about 5.5 m s^{-1}, the time response of the balloon to small horizontal scale wind perturbation was about 20 s, hence the measurement of dV/dz may be significantly erroneous. As explained in Section 5,

we have only used this part of the measurement to derive the propagation direction of the wave.

3. The data set

3.1. *The flight*

A test flight was performed on October 15, 1980 at the French Balloon Facility Base of the Centre National d'Etudes Spatiales (CNES) at Aire sur
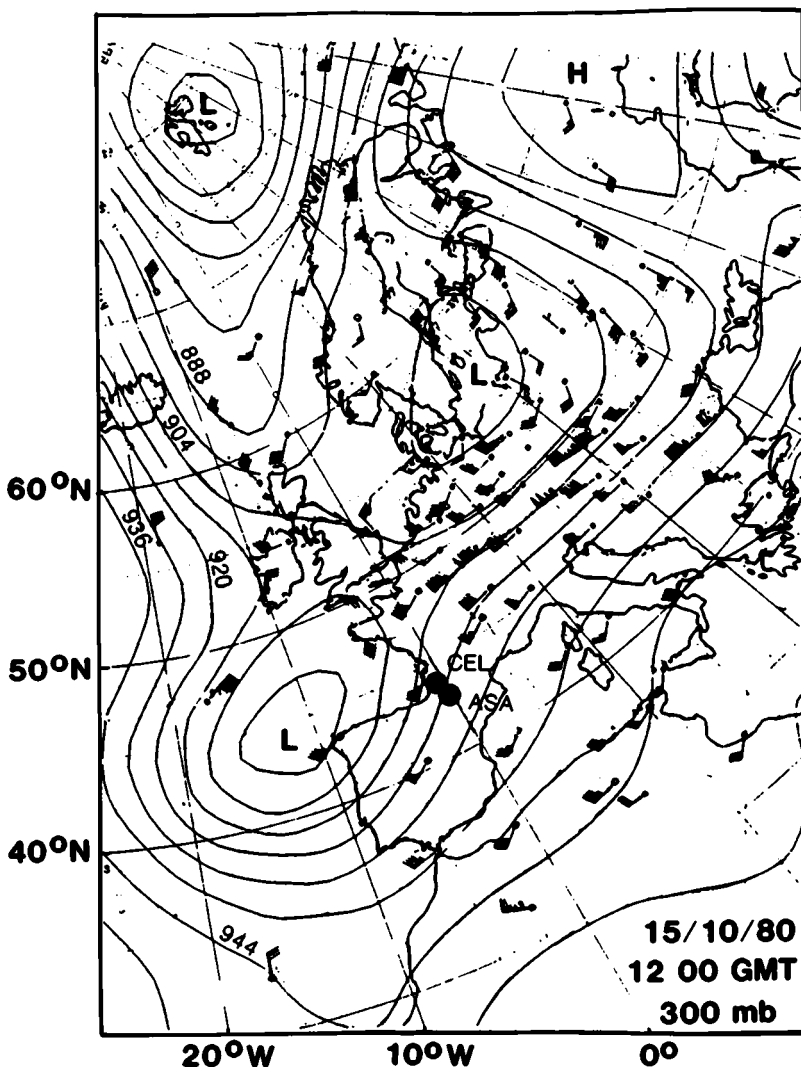

Fig. 1. Analysis 300 mb 1200 GMT October 15, 1980. The balloon launching site (ASA), and Centre d'Essais des Landes (CEL) are indicated.

l'Adour (ASA), France. The balloon, launched at 13.45 GMT reached its nominal float level (35 km) at 15.47 GMT. Due to a mechanical failure in the helisonde, no data was obtained above 28 km. During the flight, a cyclone at the surface level was centered at (10° E, 45° N). It was also present higher up in the atmosphere. The 300 mb chart at 12.00 GMT is shown in Fig. 1. We have also plotted the geographic positions of the launching site and that of the Centre d'Essais des Landes (CEL) where a wind measurement was performed at 12.44 GMT just before the flight. A SW–NE jet
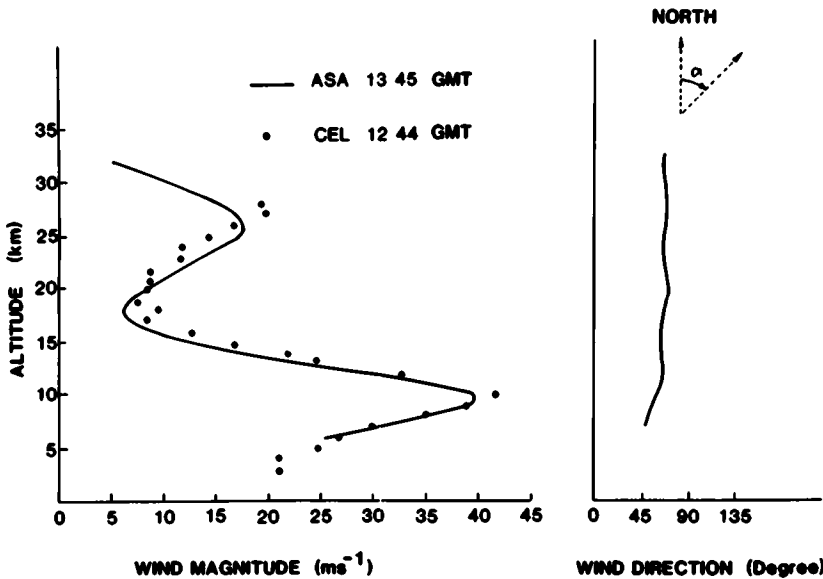
Fig. 2. Magnitude and direction of the wind measured from the tracking system of the balloon (solid line). The dots correspond to the CEL wind measurements.
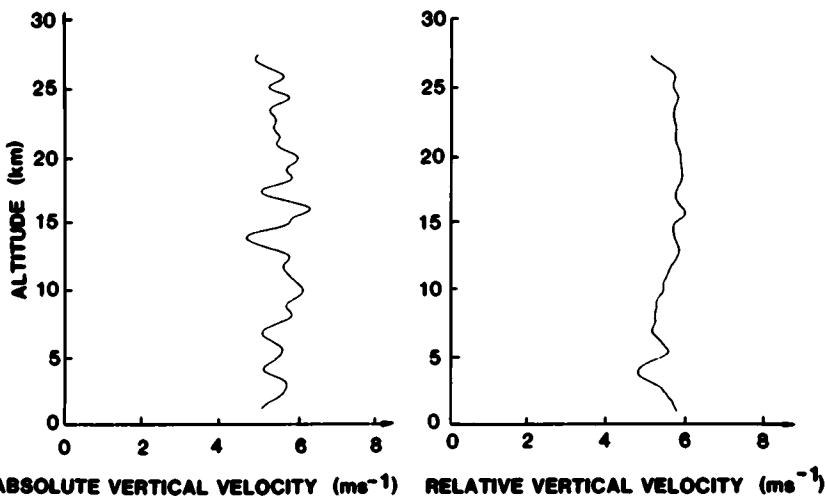
Fig. 3. (a) Vertical profile of the absolute vertical velocity W_p calculated from the pressure and the temperature measurements. (b) Vertical profile of the relative vertical velocity W_R measured with the ionic anemometer.

stream was present over the launching site and the tropopause level was at 11 km. During the ascent, the balloon was tracked by a 400 MHz telemetry system and in Fig. 2 the wind profile between 3 and 32 km is shown. We have also plotted the values obtained at CEL. We note a secondary maximum of the wind around 26 km and a remarkably constant direction for the mean flow.

3.2. Experimental results

Fig. 3a shows the profile of the velocity W_p^f. A wave-like structure with an amplitude of about 0.4 m s^{-1} is seen in the stratosphere. Its vertical wavelength is approximately 1.6 km. This variation could be due to a non-constant ascent rate of the balloon. However, the profile of the relative velocity W_R^f in Fig. 3b shows practically no corresponding fluctuations. Thus the measurements present evidence of vertical air motions.

Fig. 4a presents the vertical velocity profile W_A^f computed from eq. (5). The wave-like structure is predominant in the stratosphere, while in the troposphere it is superimposed on a large-scale vertical structure. Fig. 4b shows the temperature profile obtained by averaging the two temperature measurements. Large-amplitude fluctuations can be seen above the tropopause. Because of the strong mean temperature gradient, they are not clearly visible within the troposphere.

4. Evidence of a wave structure

4.1. Perturbation profiles

The observations of atmospheric wave motions are often complicated by the presence of multiple wave modes. In our case, the vertical profile of W_A^f in the stratosphere provides evidence of a wave structure with a well-defined wavelength. In order to separate the wave-induced velocity from the background, we have filtered the altitude series W_A^f with a running window F, l m long. We then define a perturbation velocity profile

$$W' = (1 - F_l) W_A^f. \tag{8}$$

In the calculations, we have used $l = 1600$ m and $l = 3200$ m. The results are compared in subsection 4.2. Since the mean vertical velocity in the stratosphere is small, the filtering cannot alter the W' profile, especially in the case of a non-dispersive wave. In the troposphere, however, large-scale structures (convective motions) can affect the results and, in particular, the important property $\bar{W}' = 0$ over a wavelength may not be preserved.

We have applied the same filter F to the temperature profile and we obtain
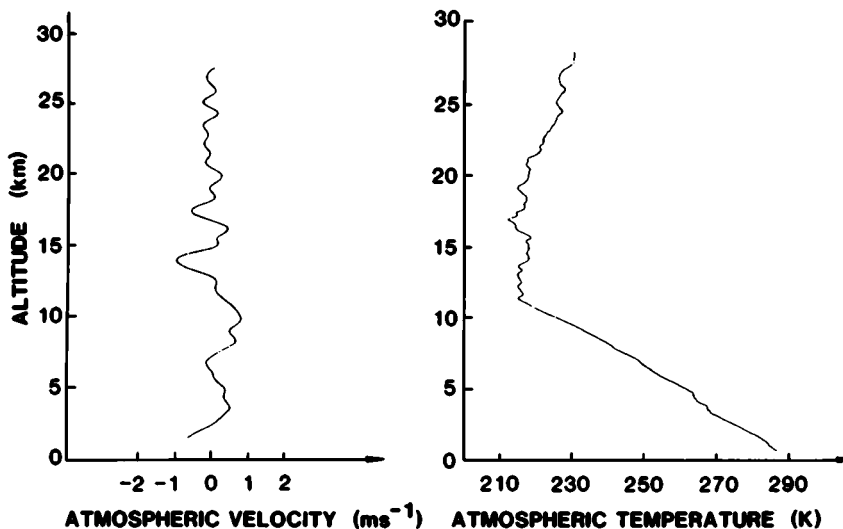
$$T' = (1 - F_l) T. \tag{9}$$

Fig. 4. (a) Vertical profile of the atmospheric velocity W_A. Note the large amplitude variations around the tropopause level. (b) Temperature profile measured along the sounding.
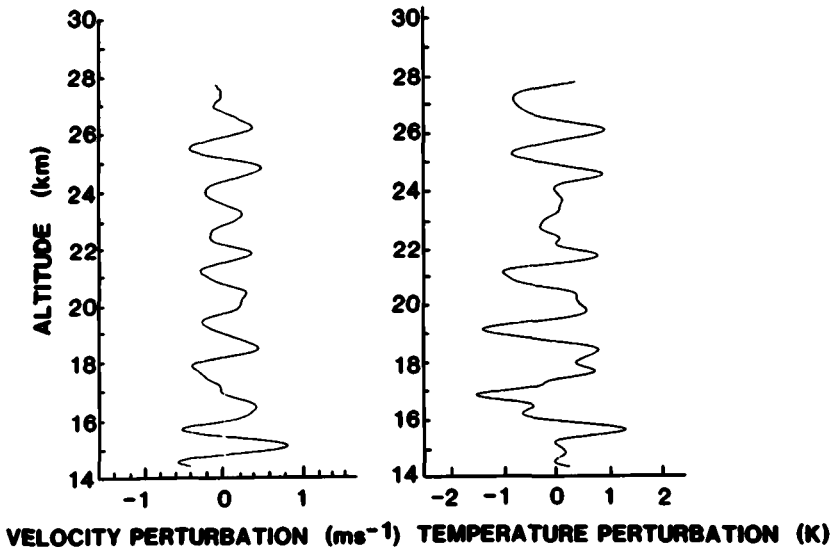
Fig. 5. (a) Vertical velocity W' and (b) temperature perturbation T' induced by the wave motion. Note the similar behaviour (amplitude and wavelength).

Errors in the temperature perturbation T' may result from the large mean tropospheric gradient. Moreover, the temperature measurement may be biased within a cloudy atmosphere and the overall error is difficult to estimate.

From the above discussion, we conclude that only the stratospheric measurements can be used directly and we present in Figs. 5a and 5b the two perturbation profiles, W' and T', computed with $l = 1600$ m above 14 km. They appear to be quite well correlated, except around 22 km.

4.2. Phase and correlation of the temperature and vertical velocity

The propagation of a gravity wave induces a relationship between velocity and temperature fluctuations. It is characterized by the correlation function

$$R(d) = \frac{\langle W'(z)\,T'(z + d)\rangle}{\langle W'^2(z)\,T'^2(z + d)\rangle^{1/2}},$$ (10)

where d is the lag distance. The maximum $R(d_m)$ of $R(d)$ gives the correlation coefficient of W' and T', and at the distance d_m the phase angle is given by

$$\Delta\Phi_{T',W'} = 2\pi\frac{d_m}{\lambda_m},$$ (11)

where λ_m, the local wavelength, is the distance between two extrema.

As a typical example, we show in Fig. 6 the function $R(d)$ averaged over a vertical interval, 2 km long, centred at 25.1 km for both $l = 1600$ m and $l = 3200$ m. We observe practically the same variation. In fact the measured phase angle must be corrected by the instrumental phase lag $\delta\Phi$ related to the time response τ of the temperature sensor by

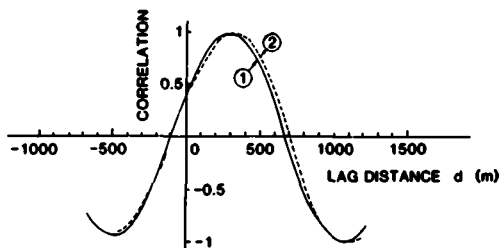$$\delta\Phi = 2\pi\frac{W_p\tau}{\lambda_m}.$$ (12)

Fig. 6. Cross correlation function of W' and T' at 25.1 km. The curve labelled (1) corresponds to a filtering over 1600 m while the curve labelled (2) corresponds to a filtering over 3200 m. The correlation coefficient is 0.98 and the phase angular difference before correction (see text) is $-70°$.

Table 1. *Phase and coherence of the wave motion*

Altitude (km)	Correlation coefficient	Actual phase angle
26.1	0.88	−84
25.6	0.95	−87
25.1	0.98	−85
24.6	1	−96
24.1	0.85	−90
23.6	very small	not measurable
23.1	very small	not measurable
22.6	0.8	+50
22.1	0.65	−45
21.6	0.85	−50
21.1	0.90	−62
20.6	0.95	−60
20.1	0.93	−70
19.6	0.92	−80
19.1	0.95	−91

In Table 1 we give the actual phase angle $(\Delta\Phi_{T',W'} + \delta\phi)$ and the correlation coefficient measured above 19 km over 13 overlapping intervals of 2 km length. The high correlation between T' and W' and the constancy of the actual phase angle allow us to conclude that a wave motion system was present during the sounding.

5. Characteristics of the wave motion

When the frequency ω of the wave is much above the inertial frequency, the polarization can be neglected if the atmosphere is taken to be stationary in the absence of waves. Along the direction x of propagation, the vertical velocity and the temperature fluctuation can be derived from the stream function ψ,

$$\psi = A\, e^{i(K_x x + K_z z - \omega t)}, \qquad (12a)$$

$$W' = \mathrm{Re}\left(-\frac{d\psi}{dx}\right) = AK_x \sin(K_x x + K_z z - \omega t), \qquad (13)$$

$$T' = -\frac{AK_x}{\omega}\left(\Gamma_a + \frac{\partial \bar{T}}{\partial z}\right)\cos(K_x x + K_z z - \omega t), \qquad (14)$$

where K_x and K_z are the horizontal and vertical wavenumbers respectively, Γ_a the adiabatic lapse

rate and A an amplitude. From eqs. (7) and (8), it follows that T' is +90° out of phase with W'.

5.1. *Direction of propagation*

As explained in Section 3, the balloon used for the test flight could not be assumed a perfect wind sensor for the induced horizontal wave velocity U'. From eq. (6) we have

$$U' = \mathrm{Re}\,(d\psi/dz) = -AK_z \sin(K_x x + K_z z - \omega t). \qquad (15)$$

Fig. 7 presents the wind intensity profile computed from

$$\vec{V}(z) = \int_{14,000}^{z} (d\vec{V}/dz')\, dz' + \vec{C} \qquad (16)$$

The altitude independent constant $\vec{C}$ has been adjusted so that $\vec{V}(z)$ equals the wind $\vec{V}_1(z)$ measured at 19,000 m by the balloon tracking system. We have also plotted $V_1(z)$ in Fig. 7 and we note the similar behaviour of the two variations. Over the 14,000 m altitude range, the integrated difference between the two measurements remains below 5 m s⁻¹. This leads to an uncertainty
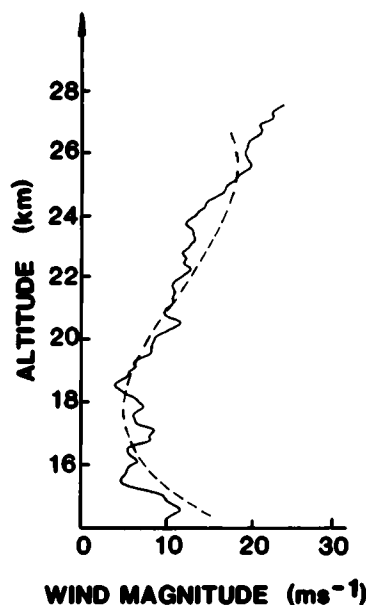

Fig. 7. Comparison between the wind magnitude profile measured directly by the tracking system (dashed line) and by the helisonde measurement (solid line). Note the slight difference over the 14,000 m altitude range.

$\delta(dV/dz)$ of about 4.10^{-4} s^{-1}. From eq. (16) we can calculate the horizontal wind fluctuations along one direction α and along the direction perpendicular to it:

$$U'_{\alpha} = (1 - F_{1600}) V_{\alpha}, \tag{17}$$

$$U'_{\perp\alpha} = (1 - F_{1600}) V_{\perp\alpha}, \tag{18}$$

where V_{α} and $V_{\perp\alpha}$ are the components along the two directions. The ratio

$$R(\alpha) = \frac{\langle V_{\alpha}^2 \rangle}{\langle V_{\perp\alpha}^2 \rangle}, \tag{19}$$

where the average is taken over the 14,000–28,000 m altitude range, is then a polarization factor and must be maximal along the direction of propagation. Fig. 8 presents the variation of $R(\alpha)$. Clearly we observe a maximum of $R = 2.1$ around $\alpha_0 = 60°$, i.e. along the jet stream flow, so that a wave propagates in this direction. However, the ratio $R(\alpha_0)$ is small and suggests an important background noise. This can be related to the

balloon behaviour and explains why we have not found a significant phase correlation between U' and W'. The result also gives evidence that the perturbation U' is small.

The results in Table 1 show that, except near 22 km where the perturbation amplitudes are very small, W' is generally $+90°$ out of phase with T'. Hence the vertical phase velocity, negative with respect to the direction of the balloon motion, is downward.

5.2. Intrinsic frequency

Using eqs. (13) and (14), the intrinsic frequency ω can be derived from

$$\omega = \frac{W'_{max}}{T'_{max}(\Gamma_a + \partial \hat{T}/\partial z)}, \tag{20}$$

where W'_{max} and T'_{max} are the perturbation amplitudes. The results are summarized in Table 2. Because of the uncertainties in the T' and W' measurements, ω lies between 0.48 and 0.33 10^{-2} s^{-1} with a mean value of 0.37 10^{-2} s^{-1} corresponding to a period of 28.5'. From the dispersion relation (asymptotic approximation)

$$\frac{K_x}{K_z} = \left(\frac{N_2}{\omega^2} - 1 \right)^{1/2}, \tag{21}$$

where $N = 2\cdot10^{-2}$ s^{-1} is the Brunt–Väisälä frequency, the ratio K_z/K_x is found to be about 6. The downward phase velocity W_Φ can be estimated directly:
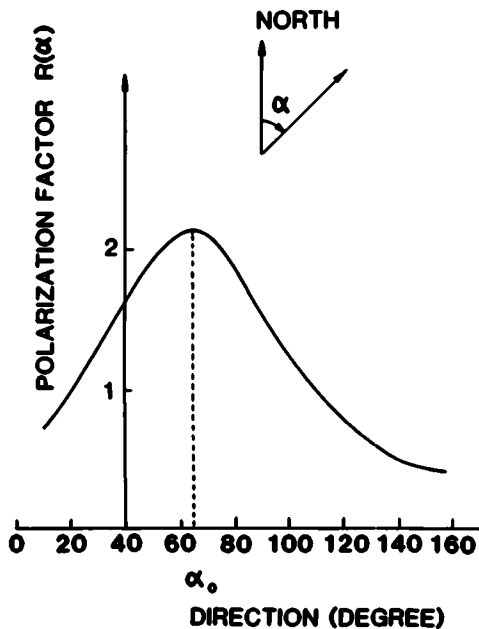

Fig. 8. Angular variation of the polarization factor $R(\alpha)$ (see text). The value α where $R(\alpha)$ is maximal corresponds to the direction of propagation of the wave, i.e. along the jet stream.

Table 2. Characteristics of the wave motion

Altitude (km)	Frequency ω (s^{-1})	Amplitude of the vertical velocity (m s^{-1})	Vertical momentum flux (N m^{-2})
25	$0.30\cdot10^{-3}$	0.42	$1.8\cdot10^{-2}$
24.4	$0.44\cdot10^{-3}$	0.44	$1.9\cdot10^{-2}$
23.6	$0.48\cdot10^{-3}$	0.49	$2.4\cdot10^{-2}$
22		0.21	
20	$0.35\cdot10^{-3}$	0.35	$3.2\cdot10^{-2}$
19	$0.37\cdot10^{-3}$	0.33	$3.1\cdot10^{-2}$
18.2	$0.32\cdot10^{-3}$	0.33	$4.2\cdot10^{-2}$
17.2	$0.32\cdot10^{-3}$	0.40	$6.8\cdot10^{-2}$
16.6	$0.35\cdot10^{-3}$	0.45	$9.0\cdot10^{-2}$
15.5	$0.31\cdot10^{-3}$	0.48	$3.5\cdot10^{-2}$

$$W_\Phi = \frac{\omega \lambda_m}{2\pi},$$ (22)

and is $W_\Phi = 0.9$ m s^{-1}, a value much smaller than the vertical velocity W_p. We can conclude that the balloon is making a nearly vertical sounding of the wave perturbations.

The actual vertical wavelength can be calculated from

$$\lambda_z = \frac{\lambda_m}{1 - W_\Phi/W_P} = 1.9 \text{ km.}$$ (23)

Thus the horizontal wavelength λ_x is about 11.5 km. For a gravity wave, the ratio of the horizontal to the vertical amplitude velocity perturbations is (eqs. (13), (14)) K_z/K_x. This leads to a small amplitude of the horizontal velocity ($\simeq 2.4$ m s^{-1}) and explains why it has not been possible to extract this parameter from our measurement below a large rising balloon.

5.3. Wave momentum flux

Gravity waves are a common occurrence in the lee of mountains. The horizontal wavelength is of the order of 10–20 km and the system is two dimensional and nearly stationary with respect to the ground. Such a configuration appears possible in the case of our observation since tropospheric wave systems are often observed with SW–NE winds in this region. All the qualitative and quantitative results reported here are quite consistent with the general characteristics of a lee wave system. Gravity waves are capable of exchanging momentum and the vertical flux of horizontal momentum is given by

$$K = \rho \overline{U' W'},$$ (24)

where the bar denotes horizontal average distance. We have explained in subsection 5.1 why it was not possible to estimate U' and consequently we cannot define the direction of the momentum flux. However, following Massman (1982) we can estimate the intensity of K as:

$$|K| = \rho \frac{N}{\omega} \overline{W'^2},$$ (25)

where the average is approximated by a vertical average over one wavelength. In Table 2 we have summarized the values of $|K|$ calculated from (25).

6. Discussion and conclusion

One of the objectives of the 1980 test flight of the helisonde was to investigate the ability of the instrument to detect gravity waves in a broad altitude range, especially in the middle stratosphere where in situ measurements are sparse. Analysis of the pressure, temperature and relative velocity data has shown that the detection of small-amplitude waves is possible up to 27 km perturbation. In the troposphere, however, some limitations arise from the presence of a high mean temperature gradient which masks the temperature fluctuations. With the actual device, it has not been possible to extract the horizontal velocity perturbation because, during the sounding, a large volume balloon cannot be assumed to be a perfect wind sensor. The next step will be to use two instrumented gondolas below the balloon in order to suppress this spurious effect. Then it will become possible to measure the direction of the momentum flux.

Despite these limitations we have observed a wave motion with a period of about 30' above a jet stream. The vertical and horizontal wavelengths were 1.9 km and 11.5 km, respectively, and there was a downward phase velocity. These characteristics are quite consistent with the presence of a two-dimensional wave in the lee of the Pyrenean mountains. While these waves have generally been assumed to be trapped in the troposphere (Lilly and Kennedy, 1973), we have provided evidence that there is a significant momentum flux in the stratosphere. The values of K that we obtain around 17 km are, however, of the same order of magnitude as those reported in Fig. 14 of the Lilly and Kennedy paper.

Massman (1981) investigated gravity waves in the lower stratosphere and found waves with a period around 30 min and a vertical velocity of 0.3 m s^{-1} which is quite comparable to the values observed by the helisonde. It is difficult to relate the two types of observations but this frequent occurrence of short-period gravity waves in the stratosphere encourages us to further develop our instrumentation and to fully investigate the wave interaction between the troposphere and the stratosphere.

7. Appendix

Time response of the microbead thermistor

The time response of the microbead thermistor can be written

$$\tau = \frac{0.66\rho C r2}{\lambda(2 + Nu)}, \qquad (A1)$$

where

ρ: density of the thermistor $(8.9 \cdot 10^3 \text{ kg m}^{-3})$,

C: specific heat of the thermistor $(3.9 \cdot 10^2 \text{ J kg}^{-1} \text{ K}^{-1})$,

λ: thermic conductivity of air $(1.95 \cdot 10^{-2} \text{ W m}^{-2} \text{ K}^{-1})$,

r: radius of the microbead $(r = 10^{-4} \text{ m})$.

In eq. (A1), Nu is the Nusselt number

$$Nu = 0.66 \text{PR}^{1/3} \text{Re}^{1/2}, \qquad (A2)$$

where Pr is the Prandlt number

$$Pr = \frac{\mu C_p}{\lambda}. \qquad (A3)$$

μ: dynamic viscosity $(1.42 \cdot 10^{-5} \text{ kg m}^{-1} \text{ s}^{-1})$,

C_p: specific heat of air at constant pressure, and Re the Reynold's number:

$$Re = \frac{2r\rho' U}{\mu}, \qquad (A4)$$

where

ρ': density of air,

U': relative velocity of the air around the thermistor.

In a wind of velocity $U = 5 \text{ ms}^{-1}$, τ varies between 4.7 s at the ground level to 19 s around 25 mb. This gives a lag distance on the temperature profile ranging from 26 m to 100 m. The effect introduces a bias phase lag $\delta\Phi$ between the temperature and the vertical velocity profiles. In Table 1, the phase difference $\Delta\Phi_{T,W}$, is corrected by the factor $\delta\Phi° = 360 \times W\tau/\lambda$.

REFERENCES

Barat, J. 1982. Some characteristics of clear-air turbulence in the middle stratosphere. *J. Atmos. Sci. 11*, 2553–2564.

Barat, J. and Génie, J. C. 1982. A new tool for the three-dimensional sounding of the atmosphere: the helisonde. *J. Appl. Meteorol. 10*, 1497–1505.

Bertin, F., Testud, J., Kersley, L. and Rees, P. R. 1977. The meteorological jet stream as a source of medium-scale gravity waves in the thermosphere: an experimental study. *J. Atmos. Terr. Phys. 40*, 1161–1183.

Chanin, M. L. and Hauchecorne, A. 1981. Lidar observations of gravity and tidal waves in the stratosphere and mesosphere. *J. Geophys. Res. 20*, 9715–9721.

Holton, J. R. 1982. The rôle of gravity wave induced dray and diffusion in the momentum budget of the mesosphere. *J. Atmos. Sci. 39*, 791–799.

Lalas, D. P. and Einaudi, F. 1980. Tropospheric gravity waves: their detection by an influence of ravinsonde balloon data. *Q. J. R. Meteorol. Soc. 106*, 855–864.

Lily, D. K. and Kennedy, P. J. 1973. Observation of a stationary mountain wave and its associated momentum flux and energy dissipation. *J. Atmos. Sci. 30*, 1135–1152.

Lindzen, R. S. 1981. Turbulence and stress due to gravity wave and tidal breakdown. *J. Geophys. Res. 86*, 9707–9714.

Massman, W. J. 1981. An investigation of gravity waves on a global scale using twerle data. *J. Geophys. Res. 86*, 4072–4082.

Matsuno, T. 1982. A quasi-one-dimensional model of the middle atmosphere circulation interacting with internal gravity wave. *J. Meteorol. Soc. Japan*, Special Issue in commemoration of the Centennial of the Meteorological Society of Japan, *60*, 215–226.

Rüster, R., Röttger, J. and Woodman, R. F. 1978. Radar measurements of waves in the lower stratosphere. *Geophys. Res. Lett. 5*, 555–558.

Uccellini, L. W. 1975. A case study of apparent gravity wave initiation of severe convective storms. *Mon. Wea. Rev. 103*, 497–513.